Heliyon

Received:
7 August 2018
Revised:
18 December 2018
Accepted:
14 January 2019

Cite as: C. Y. Tang, A. K. Zulhairun, T. W. Wong, S. Alireza, M. S. A. Marzuki, A. F. Ismail. Water transport properties of boron nitride nanosheets mixed matrix membranes for humic acid removal.
Heliyon 5 (2019) e01142.
doi: 10.1016/j.heliyon.2019.e01142

Water transport properties of boron nitride nanosheets mixed matrix membranes for humic acid removal

C. Y. Tang [a,b], A. K. Zulhairun [a,b,*], T. W. Wong [a,c], S. Alireza [a], M. S. A. Marzuki [a,d], A. F. Ismail [a,b]

[a] *Advanced Membrane Technology Research Centre (AMTEC), Universiti Teknologi Malaysia, 81310 UTM, Skudai, Johor, Malaysia*

[b] *School of Chemical and Energy Engineering, Faculty of Engineering, Universiti Teknologi Malaysia, 81310 UTM, Skudai, Johor, Malaysia*

[c] *School of Biosciences and Medical Engineering, Faculty of Engineering, Universiti Teknologi Malaysia, 81310 UTM, Skudai, Johor, Malaysia*

[d] *Hi-Tech Instruments Sdn. Bhd., Bandar Bukit Puchong, 47120, Selangor, Malaysia*

[*] Corresponding author.

E-mail address: zulhairun@utm.my (A.K. Zulhairun).

Abstract

Ultrafiltration grade polysulfone-based mixed matrix membranes (MMMs) incorporated with two-dimensional boron nitride nanosheet (BNNS) was prepared via phase inversion method. The amount of BN incorporated was varied and the influence on membrane morphology, contact angle, surface charge, as well as water permeability and humic acid rejection were investigated. Results revealed that the addition of BN to the membrane matrix resulted in profound increase in water permeability (almost tripled to that of neat PSf) and humic acid rejection due to the increase in pore size and surface negative charge. Beyond the morphological changes imparted by the inclusion of BNNS, we postulated that the presence of BNNS within the membrane matrix also contribute to the enhancement in flux and rejection based on surface-slip and selective interlayer transport. Despite the favourable augmentation of water transport and filtration performance, the MMMs suffered with fouling problem

https://doi.org/10.1016/j.heliyon.2019.e01142

due to the entrapment of foulant within the enlarged pores and the membrane valleys. Its inherent adsorptive character could be a disadvantage when utilized as membrane filler.

Keywords: Chemical engineering, Materials chemistry, Nanotechnology

1. Introduction

With technological advancement in nanotechnology, nanomaterials have demonstrated a vital role in myriad industrial applications such as electronics, automotive, food engineering, cosmetics, pharmaceuticals and environmental remediation including water purification processes [1, 2]. Nowadays, special emphasis has been made on two-dimensional layered nanomaterials. Since the isolation of graphene single-layer in 2004, graphene has been extensively characterized and engineered for various potential applications due to its exceptional electronic, thermal, mechanical, and nanofluidic properties owing to its unique atomic structure and spatial arrangement [2].

On the other hand, still little is known regarding the characteristics of boron nitride nanosheet (BNNS), a counterpart of graphene [1]. BNNS possesses identical graphitic structure to that of graphite, where all carbons are fully substituted by boron and nitrogen atoms. Despite their structural similarities, in some aspects, graphene and BNNS show quite distinctive properties from each other. Carbon based materials such as graphene and graphene oxide have been proved that hold enormous potential in water purification applications [3]. For instance, graphene may appear as black as coal, while BNNS is white, hence the nickname "white graphene" [4]. BN nanomaterials are much more chemical and thermally robust than their carbon analogues [1]. For instance, BN nanotubes (BNNTs) are highly resistance to oxidation and thermally stable up to 800 °C in contrast to carbon nanotubes (CNTs) which could not survive beyond 400 °C [5].

We can observe from recent literatures that BN nanoparticles are being actively explored in various water purification applications for the removal of oils, organic solvents and dye through adsorption technique due to their high surface area and unique B−N bonds polarity [4, 6, 7, 8, 9]. Furthermore, several computational works by molecular dynamics (MD) simulations have demonstrated that BN-based membranes possess attractive nanofluidic properties similar to that of graphene. Garnier et al [10] conducted a close investigation on the behaviour of water molecules at the interface of BNNS and graphene monolayer. The simulations revealed that solid-liquid interfacial tension on BNNS surface was lower than on graphene, and further reduced as the number of BNNS layer increased. Water molecules exhibited more favorable interactions with BNNS due to the formation of hydrogen bonds between

https://doi.org/10.1016/j.heliyon.2019.e01142

the water molecules with boron and nitrogen atoms which explain the higher water permeability transported through the BNNS pores and interlayer spacing than that of graphene. In addition, by increasing the interlayer spacing of these nanosheets (>6 Å), bulk-like property of water could be achieved during the transport hence potentially resulted in high permeation rate [11]. The high surface charge of BN nanopore could be one of the new route for the integration of BN in ionic separation and ultrafiltration applications [12]. These properties suggest that BN would be an excellent functional material for membrane development. Latest theoretical investigations also suggest that free-standing atomically thin BN membranes could efficiently reject heavy metal ions and salts for seawater desalination [13, 14].

However, fabricating free standing BN membranes could impose a considerable challenge in terms of fabrication technique, reproducibility, and mechanical stability of the inorganic membrane. Preliminary attempt on exploring the applicability of BN nanomaterials for water filtration could be realized by preparing BN-based mixed matrix membranes (MMMs). Therefore, we report for the first time, the preparation and characterization of mixed matrix ultrafiltration membrane incorporated with BNNS particles. The effects of BNNS on the membrane morphology and physico-chemical properties are presented. Humic acid (HA) which often exists in water bodies was chosen as the model pollutant for the evaluation of the membrane filtration performance. Finally, in depth discussion on the microstructural properties of BNNS and how it affects the selective permeation and water transport through BNNS MMMs are provided.

2. Materials and method

2.1. Materials

Boron nitride nanosheet (~1 μm, 98% BN) (10043-11-5) purchased from Sigma-Aldrich was used as the membrane filler for this study. Polysulfone Udel® P-3500 in pellet form (Solvay) (25154-101-2), poly(ethylene glycol) (PEG 400, M_n = 400 g/mol, Sigma-Aldrich) (25322-68-3), N-methyl-2-pyrrolidone (NMP) (872-50-4) were used as the main polymer, pore forming agent and the solvent for preparing the membrane dope solution. Humic acid (Sodium salt, tech., 50−60% as humic acid, 2 kDa−500 kDa) (68131-04-4) procured from Acros Organics was used as the model pollutant. Hydrochloric acid (HCl, 10%, Merck) (7647-01-0) was used for membrane washing in fouling study.

2.2. Fabrication of PSf/BN membranes

Flat sheet PSf/BN membranes were prepared by phase inversion technique. Five different PSf/BN membranes were fabricated according to the dope solution as formulated in Table 1. Briefly, a predetermined amount of PEG and BN were added

https://doi.org/10.1016/j.heliyon.2019.e01142

Table 1. Dope formulation of the casting solutions containing different amount of BN.

Membrane	Dope formulation (wt %)			
	PSf	PEG 400	BN	NMP
PSf	15	2	0	83.0
PSf/BN 0.5	15	2	0.5	82.5
PSf/BN 1.0	15	2	1.0	82.0
PSf/BN 1.5	15	2	1.5	81.5
PSf/BN 2.0	15	2	2.0	81.0

to the NMP solution, followed by 1 hour of ultrasonication. PSf pellet was then added to the suspension under vigorous mixing for the next 24 hours, producing homogeneous casting solution. Prior to casting, the prepared solution was then sonicated for another 1 hour to remove trapped air. The membranes were evenly spread ($\sim$100 μm) on a smooth glass plate using glass rod. The nascent membrane was immediately quenched in a water bath (25 $\pm$ 2 °C) to initiate the phase inversion process. Next, the membrane was peeled off from the glass plate and kept in a separate water bath for the next 24 hours to remove the residual solvent. The membrane was dried in oven (60 $\pm$ 2 °C) and subsequently used for permeation tests and characterizations.

2.3. Characterizations

2.3.1. BN characterizations

The morphology of BN particles was examined using transmission electron microscopy (TEM Hitachi HT7700) operated at the transmission mode of 100 kV. BN crystal structure was investigated by X-ray diffraction (XRD) analysis (Siemens D5000 Difractometer), with Cu-Kα radiation (λ = 0.1541 nm), operated at 30 mA and 40 kV from 3° to 80° at increment rate of 0.05°/min. N_2 adsorption isotherm was obtained by Surfer Gas Adsorption Porosimeter (Thermo Fisher Scientific Inc.) and the specific surface area of BN was determined by Brunauer, Emmett and Teller (BET) method. The volume of gas adsorbed to the surface of the particles was measured at the boiling point of nitrogen, $-$196 °C. BN sample was then degassed at 250 °C for 12 h with the increment step of 10 °C/min.

2.3.2. Membrane characterizations

The morphology of membrane's surface and cross-sectional area were inspected using scanning electron microscopy (SEM, Hitachi TM3000 Tabletop Microscope). The membrane was cryo-fractured inside liquid nitrogen to ensure smooth cross-sectional break. The membrane was mounted on stainless steel stub using carbon tape, followed by a brief gold-sputtering step prior to imaging.

https://doi.org/10.1016/j.heliyon.2019.e01142

Topological properties of the membranes were investigated using atomic force microscopy (Hitachi AFM 5100N). The membrane surface (1 μm × 1 μm) was scanned using non-contact mode. The average roughness (R_a), the root mean square of Z data (R_q) and the mean difference between the highest peak and lowest valleys (R_z) were measured.

Contact angle (CA) measurement was conducted by sessile-drop method employing an automated CA goniometer (OCA 15 pro, DataPhysics) using RO water as probe liquid. Ten measurements were recorded at multiple points of each membrane sample and the mean value was determined.

The zeta potential of the membrane was analyzed by electrokinetic analyzer (Anton Paar SurPASS) equipped with an adjustable gap cell based on streaming potential and streaming current measurement. 1 mM of KCl was used as the background electrolyte and the pH was varied from 2 to 11 using 0.1 M of HCl and 0.1 M of NaOH. A maximum pressure of 400 mbar was applied to induce laminar flow. The zeta potential was calculated based on the Helmholtz-Smoluchowski approach.

2.4. Average porosity and mean pore radius of membrane

In order to determine the mean pore radius of the membrane, the porosity of the membrane was first evaluated via gravimetric analysis. The membrane was soaked in water (25 ± 2 °C) for 24 h. The membrane-wet surface was gently wiped with soft tissue paper and weighed. The membrane was then dried in oven (60 °C) until constant weight was observed. The overall porosity, ε of the membrane was calculated based on the following equation:

$$\varepsilon = \frac{\left(w_{wet} - w_{dry}\right)\rho_w}{\left(\left(w_{wet} - w_{dry}\right)/\rho_w\right) + \left(w_{dry}/\rho_p\right)} \times 100 \quad (1)$$

where W_{wet} and W_{dry} represent the weight of wet membrane (g) and the weight of dry membrane (g), respectively, p_p is the density of the polymer (1.24 g/cm^3), and p_w is the density of water (g/cm^3). The mean pore radius (r_m) of the membrane was determined via filtration velocity method based on Guerout-Elford-Ferry equation:

$$r_m = \sqrt{\frac{(2.9 - 1.75\varepsilon) \times 8\eta \mathrm{lQ}}{\varepsilon \times A \times \Delta \mathrm{P}}} \quad (2)$$

where η is the water viscosity (8.9×10^{-4} Pa.s), l is the membrane thickness (m), Q is the volume of the permeate water per unit time (m^3 s^{-1}), A is the effective surface area of the membrane (m^2), and ΔP was the trans-membrane pressure (bar).

https://doi.org/10.1016/j.heliyon.2019.e01142

2.5. Permeation properties of PSf/BN membranes

All permeation experiments were conducted using a custom-built cross-flow permeation cell. The effective membrane surface area tested for permeation was 14.6 cm^2. The pure water flux (PWF) of the membranes were measured at 1 bar. The membrane was first compacted at higher pressure (2 bar) until constant flow was observed to eliminate the compaction effect. PWF was determined using the following equation:

$$J_{WF} = \frac{V}{A\Delta t} \tag{3}$$

where J_{WF} is the water flux (L/m^2 h), V is the volume of water permeated across the membrane (L), Δt is the time taken for collecting the permeate (h) and A_m, is the effective membrane area (cm^2).

Humic acid (HA) solution of 1000 ppm was tested for rejection studies. UV-visible spectrophotometer (HR-5000) at a wavelength of 545 nm was used to measure the concentration of HA. The rejection efficiency, $R(\%)$ was calculated based on the following equation:

$$R(\%) = \left(1 - \frac{C_p}{C_f}\right) \times 100 \tag{4}$$

where C_p and C_f are the solute concentration (ppm) in the permeate and feed, respectively. All filtration experiments were operated at 1 bar and 25 $\pm$ 2 °C. In order to assess the stability of filtration performance of the fabricated membranes, HA permeation experiment was extended for 180 min. The permeate was periodically collected every 10 min. The flux recorded after 180 min was denoted as J_{cp}. The membrane was then rinsed with water to remove the concentration polarization (CP) layer for 10 min. The pure water flux was measured again which denoted as J_c. Lastly, 0.1 M of HCl aqueous solution was used to wash the membrane for 10 min and the PWF was measured again, and denoted as J_a.

3. Results and discussion

3.1. Characterization of BN

TEM images in Fig. 1 reveal the shape of BN particle used as the membrane filler for this study. One may describe its morphology as resembling to that of graphene; two-dimensional, disk-shaped particle of very high aspect ratio. Its diameter ranges from a few hundreds to 1000 nm in agreement with the suppliers' specification. Note that, the individual BN nanosheet is very thin, 0.45 nm thick for a monolayer BN [15]. Most BN particles are observed to be stacked on top of one another; hence they appeared darker in the image. The interlayer distance between each stacking layer also

https://doi.org/10.1016/j.heliyon.2019.e01142

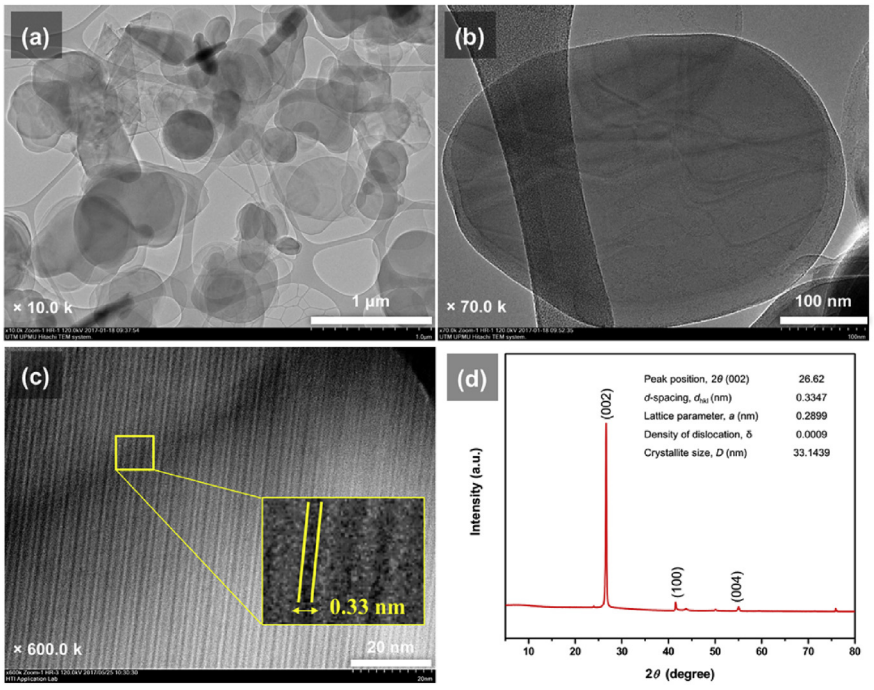

Fig. 1. TEM images of BN nanosheets at (a) low magnification, 10.0 k times; (b) higher magnification, 70.0 k times (c) measurement of the basal spacing; and (d) the corresponding XRD pattern.

can be determined from XRD analysis. XRD spectrum of BN nanosheets in Fig. 1d demonstrates three significant diffraction peaks at 2θ of 26.62°, 41.50°, and 55.02°, which correspond to (002), (100), and (004) plane, respectively. The peaks matched to hexagonal BN (*h*-BN) structure and in good agreement with the standard spectrum (JCPDS No.: 00-034-0421) [16] implying good BNNS quality. From the XRD data, crystalline properties of BN nanosheets are calculated and summarized in the same figure. The interlayer distance measured from the d_{002} of 26.62° revealed a 0.33 nm spacing, in agreement with the measurement from the TEM image (Fig. 1c). This interlayer spacing has been accounted as an important feature which determine the molecular transport and adsorption properties of BN particles [4, 6] similar to GO [17]. Very small value of density of dislocation, δ indicates that the nanosheet has low atomic defect and is highly crystalline, hence low porosity. The N_2 adsorption test revealed that the specific surface area of BNNS filler was only 23.81 m^2/g, which corroborate its low porosity characteristic.

3.2. Membrane characterizations

Fig. 2 shows the surface and cross-sectional morphology of the membranes fabricated in this study. All membranes were fabricated by phase inversion method hence their cross-section displayed the typical asymmetric structure with finger-like morphology while the active skin layer on the top surface was densely covered

https://doi.org/10.1016/j.heliyon.2019.e01142

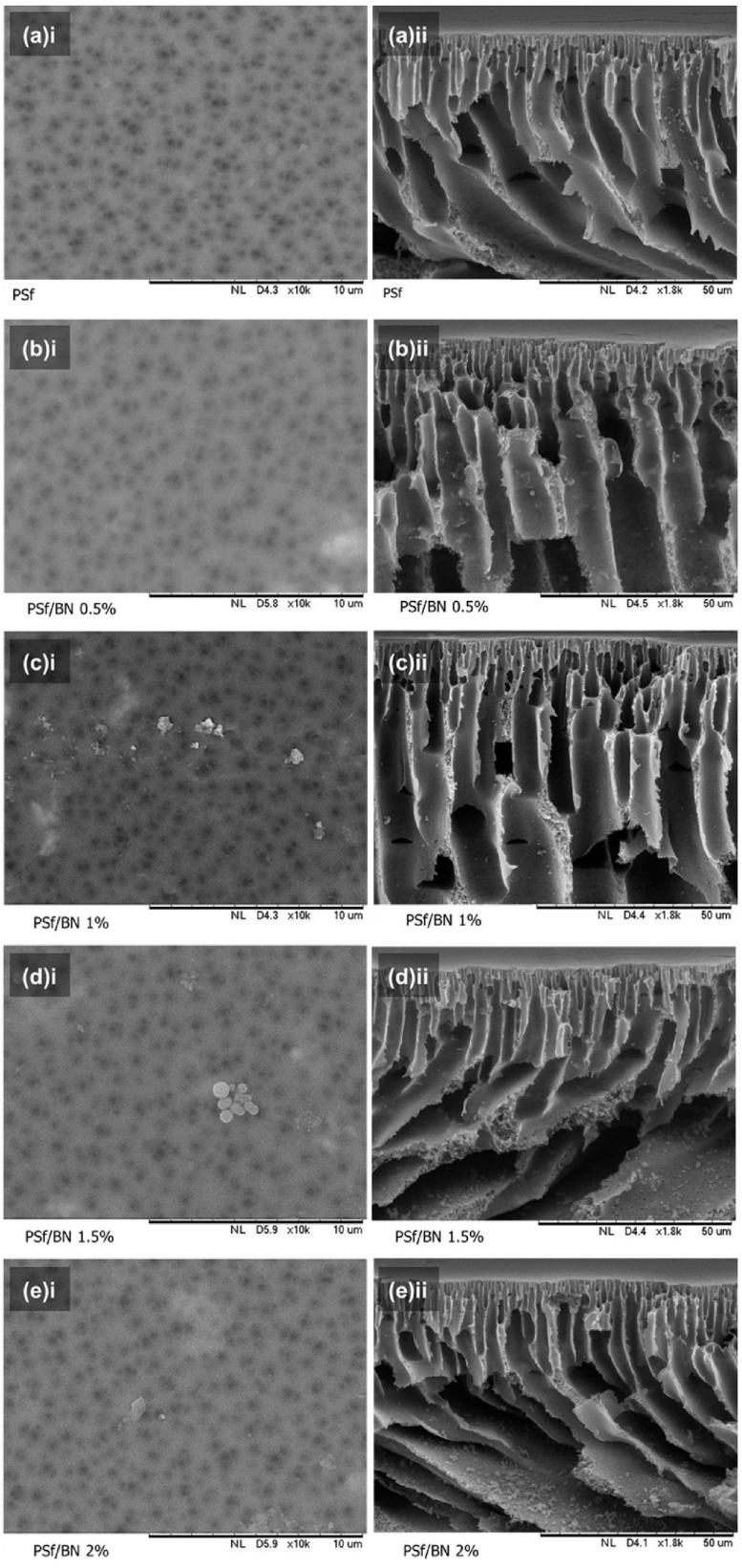

Fig. 2. SEM images for (a) PSf membranes, (b) PSf/BN 0.5%, (c) PSf/BN 1.0%, (d) PSf/BN 1.5%, and (e) PSf/BN 2.0% (i: surface; ii: cross-sectional morphology).

https://doi.org/10.1016/j.heliyon.2019.e01142

with pores [18]. The incorporation of PEG tends to increase the exchange rate in between additive and non-solvent, resulting in the formation of macrovoids [19]. Based on the SEM images, the addition of BNNS to the casting dope has only resulted in monotonous change in the overall morphology. Considering its atomically thin, high aspect ratio structure, BN layers would preferentially orient themselves horizontally, parallel to the membrane surface. Therefore, finding the BNNS filler from the cross-sectional view would be a challenging task. This also suggested that BN filler was homogeneously dispersed throughout the membrane matrix. However, from the plane view of the membrane we were able to observe a mild degree of particle agglomeration on the membrane surface as the filler loading exceeded 1%. Fig. 2d(i) shows the presence of disk-shaped particles on the surface of PSF membrane loaded with 1.5 wt.% of BN.

The membrane's morphology was further characterized in terms of the porosity and the mean pore radius as summarized in Table 2. The measured pore size fell within the ultrafiltration range (10−100 nm). In general, we can see that both parameter gradually increased with increasing BNNS loadings. Such trend has been constantly reported in the literature [20]. This phenomenon could be ascribed to the interfacial stresses between the polymer chains and the filler occur during the phase inversion process which leads to the formation of larger pores and more opened substructure [20].

Fig. 3 shows the AFM images of the active membrane surface of the neat PSf and PSf/BN 1.0% MMM. The surface roughness parameters: average roughness (R_a), root mean square of the Z data (R_q), and average distance between the highest peak and lowest peak valley (R_z) are inserted in the figure. The incorporation of BNNS into the membrane resulted in the formation of smaller and more polymer nodules, hence increasing the average roughness of the membrane surface (higher R_a and R_q). The increase in the number of polymer nodule might be attributed to the interaction between the polymer chain and the flat BNNS surface. Polymer chains tend to be adsorbed onto the particle surface and conformed according to the BN smooth surface into smaller nodules upon precipitation. Note that the creases and valleys became deeper (R_z of the MMM was higher) upon the inclusion of BNNS with might be a concern associated to fouling.

Table 2. Average porosity and the mean pore radius.

Membrane	Average porosity (%)	Mean pore radius (nm)
PSf	55.36 ± 1.69	17.28 ± 1.46
PSf/BN 0.5	65.03 ± 1.58	18.65 ± 1.34
PSf/BN 1.0	68.45 ± 2.01	22.20 ± 1.88
PSf/BN 1.5	76.78 ± 1.91	20.66 ± 1.79
PSf/BN 2.0	76.78 ± 2.24	23.75 ± 2.11

https://doi.org/10.1016/j.heliyon.2019.e01142

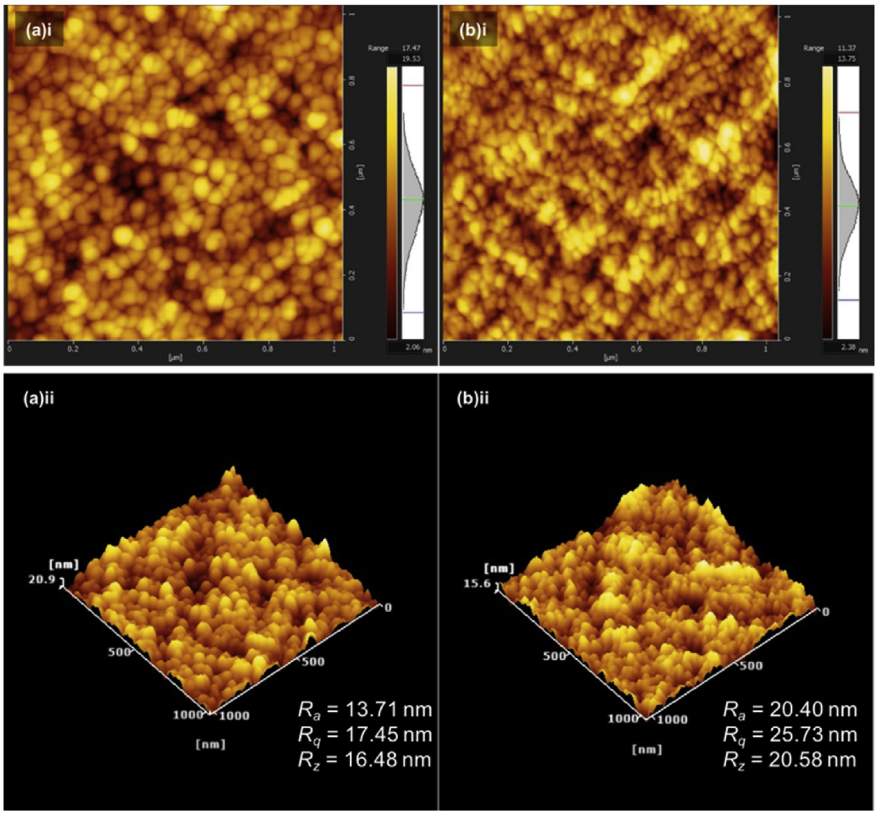

Fig. 3. Topo (top) and 3D (bottom) AFM images for (a) neat PSf membrane, and (b) PSf-BN 1.0%. Scan size 1 μm × 1 μm.

Contact angles play an important role in the mass transfer at the membrane surface. Fig. 4 shows the measured surface contact angle of the membranes as a function of BN loadings. The results show that the contact angle of the membranes consistently decreased from 78° for the neat PSf membrane to 64.5° as the filler added up to 2 wt.%. Although the intrinsic water contact angle of BNNS monolayer was reported to be fairly hydrophobic ~80° [21], BNNS filler was incorporated within the polymer matrix and hence did not interact directly with water. We can imply that the increase in membrane porosity and the enlargement of the pore size imparted greater influence on the membranes' contact angle rather than the hydrophobicity nature of BNNS filler. In addition, based on the surface roughness data, BN-filled membrane possesses relatively rougher surface. Rougher surface will increase the effective surface area of membrane hence decrease the interfacial contact angle.

3.3. Transport properties of PSf/BN MMMs

3.3.1. Water transport through PSf/BN MMMs

Filtration experiments were conducted as the performance indicator for the fabricated membranes. Distilled water was used in the experiment to determine the effect

https://doi.org/10.1016/j.heliyon.2019.e01142

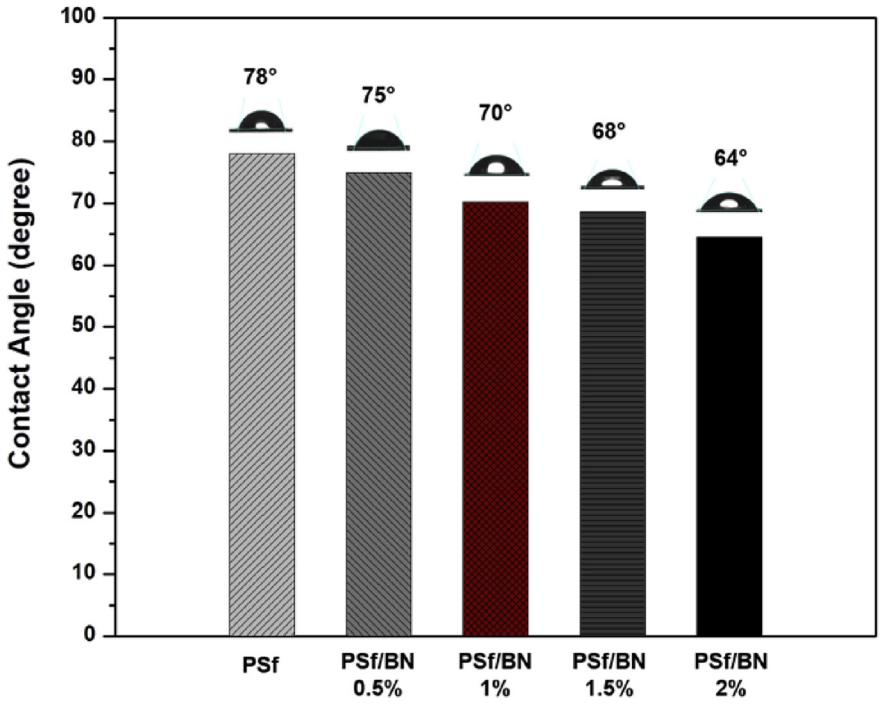

Fig. 4. Contact angle of PSf membrane with different BN loadings. The mean values presented have standard deviation of ±2°.

of BNNS incorporation on its permeation properties. As one could expect from the results of prior characterizations, the increase in pore size, total porosity, and reduced contact angle would result in membranes with enhanced water fluxes as shown in Fig. 5. Neat PSf membrane had a PWF of 50 L/m^2.h.bar. Note that the flux increased to 80 and 110 L/m^2.h.bar for PSf/BN 0.5% and PSf/BN 1%, an increment of 60% and 120%, respectively. As the BN filler content increased to 1.5 wt.%, instead of observing a 180% flux improvement, PWF slightly increased to 120 L/m^2.h.bar, which is merely 140% enhancement. When the loading was further increased to 2 wt.%, the slope in PWF enhancement relative to PSf/BN 1.5% was much higher in comparison to the enhancement observed for neat PSf to PSf/BN 0.5%, and from PSf/BN 0.5% to PSf/BN 1%. If water permeation rate were to be solely correlated to the pore size of the membrane, the PWF should proportionally increase according to the same slope. The increase in pore size was ~37% (from 35 nm to 48 nm) as the loading increased from 0 to 2 wt.%, which might account for the dramatic increase in water flux. However, there should be a more delicate explanation to these phenomena but has been frequently undermined.

For instance, often times in the literature, particularly related to mixed matrix membranes, once we found the pore size, porosity, and contact angle data seemed to favour our flux measurement, we may jump to a premature conclusion that the filler had improve the surface morphology, hence improve the permeation properties of

https://doi.org/10.1016/j.heliyon.2019.e01142

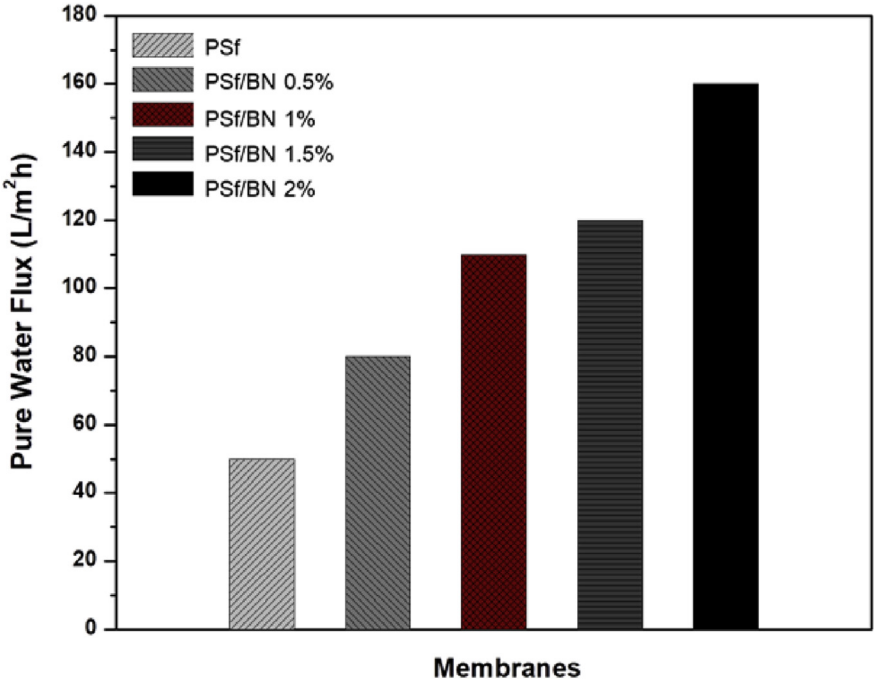

Fig. 5. Pure water flux of PSf membrane with different BNNS loading. The mean values presented have standard deviation ±2%.

the membranes. No matter how compelling the data might be, we should not neglect the fact that water molecules and the solutes it carries have to travel through a "mixed matrix" − a complex maze made up of intertwining polymer chain filled with foreign inorganic particles. Considering this, molecular transport through a mixed matrix membrane would be significantly affected by the geometry of the discreet phase and how they conform themselves in the polymer matrix [22].

In order to explain our PWF data, we must recall that BNNS has a disk-like shape, with an average diameter of ~400 nm. Atomically thin BNNS layers are stacked layers upon layers like a deck of filter paper held together by weak van der Waals interactions. This deck of BNNS layers is not easily exfoliated in normal mixing conditions due to its low surface energy [23]. The *D*/*L* ratio is very large; hence it is rational to assume that majority of the sheets will be oriented parallel to the membrane surface as they were incorporated in the polymer matrix. Consider that these BNNS layers are homogeneously spread throughout the membrane matrix, some of which will present at the top skin layer region beneath the pores (for the case of PSf/BN 0.5% and PSf/BN 1%). Due to large surface-to-volume ratio, as water molecules enter the membrane pores, water molecules will likely to encounter the BN particles. Through MD simulations, Garnier et al. [10] revealed that the water molecules preferentially bounded to BNNS surface (high wetting feature) and subsequently slide along the surface or slipped on the hydrogenated edges. High crystallinity of BNNS and smooth surface could assist the surface slip mechanism.

https://doi.org/10.1016/j.heliyon.2019.e01142

In addition, the empty spaces between BNNS layers will act as conduit for additional pathways for molecular transport. Within this sub-nanometer conduit, water structure is confined and behaved significantly different than that in the bulk [24]. Diffusion plays a vital role in water transport in confined environments. Water diffusion through nanochannels was characterized as anomalously fast, up to 1 meter per second which attributed to frictionless molecular transport, high capillary pressures (about 1,000 bar) and large slip lengths similar to that of graphene interlayer, carbon nanotubes and biological nanopores [25, 26] Furthermore, the adsorption of polymer chain onto the surface of BN sheets upon mixing and phase inversion was highly probable [22]. The adsorbed polymer would intercalate, consequently expand the interlayer spacing by overcoming the van der Waals forces. An increase in BNNS interlayer spacing up to 8 Å would lead to a substantial increase in water permeability, 150% higher than that of permeation through a 3.3 Å intrinsic interlayer gap [9]. Furthermore, bulk-like water transport with ballistic diffusion would occur as BNNS interlayer spacing increases [11]. Fig. 6 illustrates the possible selective permeation phenomenon through the membrane pore, surface slip and molecular transport through the BNNS interlayer.

When the BNNS loading was increased to 1.5 wt.%, as can be seen from the SEM images (Fig. 3(d)i), BN particles started to agglomerate and were found on the membrane surface. These particles may block the pores accessible for water permeation, as a consequence, the number of active pores was reduced. Although the water flux

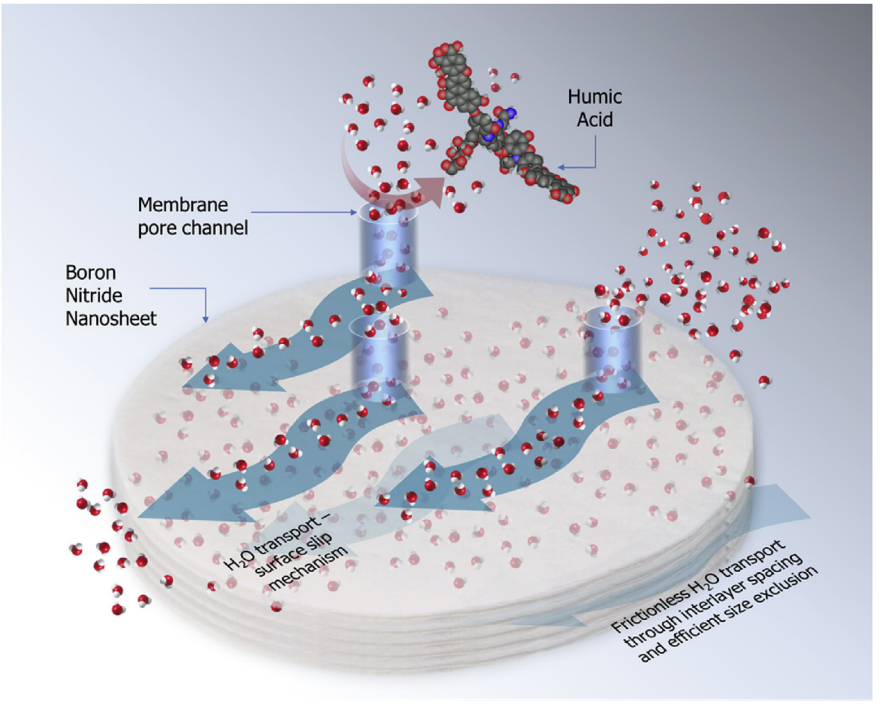

Fig. 6. Illustration of water transport mechanism at the membrane pore, BNNS surface, and through the interlayers.

https://doi.org/10.1016/j.heliyon.2019.e01142

measured still higher than PSf/BN 1%, it was lower than the projected flux. This explains why the average pore radius calculated for PSf/BN 1.5% was lower than that of PSf/BN 1%. Further filler loading increment demonstrated a steep increase in the pure water flux. However, the increase in water flux could be ascribed to the presence of less-selective voids between the filler and the polymer matrix due to a higher degree of filler agglomeration. These voids would adversely affect the rejection capability of the membranes.

3.3.2. Humic acid rejection of PSf/BN MMMs

HA rejection data demonstrated in Fig. 7 corroborates the less-selective effects of PSf/BN 1.5% and PSf/BN 2% due to the filler agglomeration. The HA rejection for PSf/BN 1.5% and PSf/BN 2% was 82% (±1%) and 70% (±2%), respectively. Meanwhile, PSf/BN 0.5% and PSf/BN 1% had shown an appreciable increase in HA rejection. Neat PSf membrane rejected 90% of HA, while PSf/BN 0.5% and PSf/BN 1% improved the rejection to 92% (±0.5%) and 94% (±0.5%), respectively. Although, the improvement in rejection was somewhat marginal, given that these membranes had also improved the membrane performance in terms of water flux, BNNS should be regarded as an interesting choice of membrane filler.

The rejection of HA substance in the water would be predominated by size exclusion mechanism. The molecular weight of sodium salt HA used for the filtration

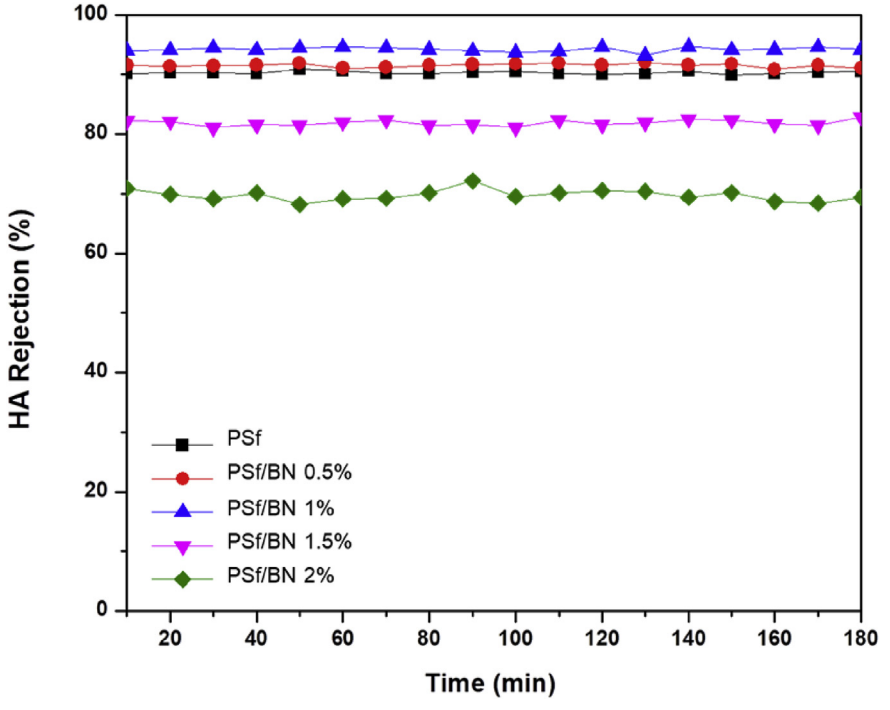

Fig. 7. Humic acid (1000 ppm) rejection profile measured over a 3 h period. Filtration was conducted at 1 bar and 25 ± 2 °C.

https://doi.org/10.1016/j.heliyon.2019.e01142

experiment ranged from 2 kDa to 500 kDa, while the average pore diameter of the fabricated membranes ranged from 35 nm to 48 nm. These pore size range would be efficient to reject solutes having molecular weight higher than 70 kDa (based on pore size-molecular weight cut-off correlation), but not reject the rest of smaller solutes. As per our previous discussion, again, the interlayer spacing of BNNS could be playing an interesting role in molecular transport and separation. Besides transporting water molecules through the interlayers, these regularly-spaced nanosheets may act as additional sieve for rejecting the remaining HA of small molecular weight inside the membrane matrix. The intrinsic basal spacing of BNNS is smaller than 1 nm, hence 2 kDa and larger HA could not possibly traverse through the layers. The presence of the BNNS particles throughout the membrane may reinforce the matrix selectivity by creating a tortuous path for solute transport.

In addition, the zeta potential measurement revealed that the presence of BNNS in the membrane also had significant impact on the membrane surface charge. Fig. 8 demonstrates the surface zeta potential of the neat PSf membranes and PSf/BN 1% MMM with respect of pH. The isoelectric point of the membrane had shifted to a lower pH value with the addition of BNNS: from pH 5 for neat PSf, to pH 4.1 for PSf/BN 1%. The increase in negative surface charge could be ascribed to the inherent polarity of BNNS particles. Singla et al. [16] reported the zeta potential value for BNNS was -59 mV. Since HA contains acidic functional groups, under increasing pH condition, deprotonation will cause the molecules to exhibit a negative surface charge too [27]. Under these circumstances, the enhanced electrostatic

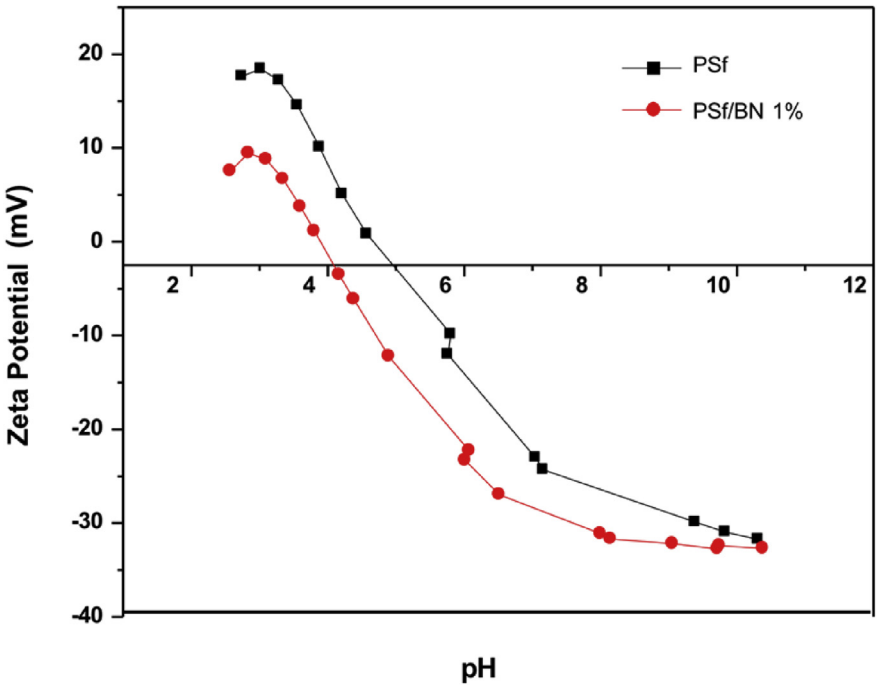

Fig. 8. Zeta potential of membrane surface as a function of pH.

https://doi.org/10.1016/j.heliyon.2019.e01142

repulsion forces between the membrane and HA may impart fair contribution to the rejection improvement.

3.4. Fouling phenomena

Besides pure water permeation and HA rejection experiments, HA filtration experiment was conducted to assess the stability of permeation flux of the fabricated membranes. The permeation flux profile over 180 min of filtration is shown in Fig. 9. As one would expect, the membranes permeation flux would be decreasing as a function of time which associated to concentration polarization and cake layer formation. However, it was to our surprise that BN-filled membranes demonstrated greater drop in flux despite the favourable improvement in their surface charge. For instance, PSf/BN 1.0% suffered a 56% flux reduction after 180 min of filtration, while the neat membrane lost about 50% of permeation flux. On the other hand, PSf/BN 2.0% had the least flux loss, sustaining approximately 74% of its initial flux. Referring to Table 3, the flux recovery of all membranes after flushing with RO water (J_c/J_{WF}) was just slightly improved. While, after chemical cleaning with 0.1 M of HCl aqueous solution, the flux recoveries (J_a/J_{WF}) were increased to 70% for PSf, 63% for PSf/BN 0.5%, 60% for PSf/BN 1.0%, 61% for PSf/BN 1.5%, and 82% for PSf/BN 2.0%.

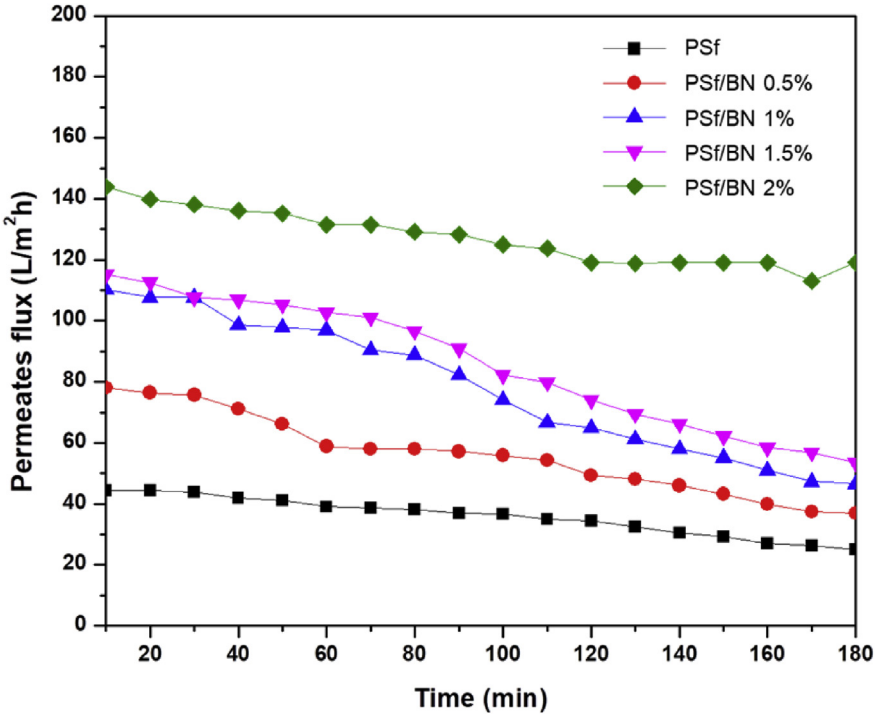

Fig. 9. Humic acid (1000 ppm) filtration profile measured over a 3 h period. Filtration was conducted at 1 bar and 25 ± 2 °C.

https://doi.org/10.1016/j.heliyon.2019.e01142

Table 3. Flux of membrane throughout the HA filtration process.

Membrane	J_{WF}	J_{cp}	J_c	J_a	1-J_{cp}/J_{WF}	J_c/J_{WF}	J_a/J_{WF}
PSf	49.32	25.07	30.00	34.52	0.49	0.61	0.70
PSf/BN 0.5	82.19	36.99	45.62	51.37	0.55	0.56	0.63
PSf/BN 1.0	114.25	46.44	53.84	69.04	0.59	0.47	0.60
PSf/BN 1.5	121.23	53.43	64.11	73.97	0.56	0.53	0.61
PSf/BN 2.0	160.28	119.18	127.40	131.51	0.26	0.79	0.82

J_{WF} is the pure water flux; J_{cp} is the flux recorded after 180 min; J_c is the flux recorded after washing with RO to remove the concentration polarization (CP) layer; J_a is the flux after washing with 0.1 M of HCl aqueous solution to remove adsorbed foulant; 1-J_{cp}/J_{WF} is flux reduction after 180 min filtration; J_c/J_{WF} is the recovery after RO washing; J_a/J_{WF} is the recovery after washing with 0.1 M of HCl aqueous solution.

These fouling phenomena could be ascribed to the entrapment of humic substance within the enlarged pores and the membrane valleys. As demonstrated earlier, it was shown that the average pore size of the membranes and the depth of the surface valley were increasing as a function of BNNS loadings. Without any improvement in surface chemistry i.e., hydrophilicity, the tendency for cake formation on the membrane surface would increase. However, as the pore size grew, the foulant could pass through the pores to the permeate site. This explains why PSf/BN 2% did not fouled as much as the other membranes.

From these results, it is apparent that the incorporation of BNNS into the membrane does not endow anti-fouling character towards humic acid, yet fouling become more severe. In addition, humic acid that used in this work contains sodium salt that will increase the polarity of the solution. BNNS nanoparticles are in fact an excellent adsorbent for various organic pollutants predominantly due to its B-N bonds polarity which would favour the transfer of electrons with the aromatic organic molecules leading to physisorption reaction [5]. With the present of sodium salt (common cation in all cases was Na^+), anions could increase the adsorption capability of the humic acid onto the membrane [28]. It seems that one of its advantages had turned out to be a drawback if it were to be incorporated in the membrane matrix without prior modification. For future development of BN-based MMMs, we speculate that the surface chemistry of the particle needs to be modified in order to reduce the physisorption. That way, the enhancement in water flux and solute rejection of the membrane would not be burdened by a long-term fouling issue.

4. Conclusion

In this study, we have demonstrated a practical use of BNNS as the filler for improving the performance of ultrafiltration membranes. Being atomically thin, homogenous dispersion within polymer matrix could be achieved up to ~1wt.% loading. BNNS incorporation have resulted in membranes with larger pore and

https://doi.org/10.1016/j.heliyon.2019.e01142

porosity which lead to the improvement in water flux. We also inferred that BNNS two-dimensional multi-layered structure was playing a unique role in enhancing water transport and endowing selective molecular permeation. However, we have also learned that due to the adsorptive nature of BNNS, fouling was inevitable probably due to its strong adsorptive nature. We believe that BNNS would serve as a unique material in water purification application if the adsorptive nature of the particle could be specifically tailored, while providing frictionless water transport through its interlayer with controlled spacing.

Declarations

Author contribution statement

C.Y. Tang, A.K. Zulhairun: Conceived and designed the experiments; Performed the experiments; Wrote the paper.

T.W. Wong, A.F. Ismail: Contributed reagents, materials, analysis tools or data.

S. Alireza, M.S.A. Marzuki: Analyzed and interpreted the data.

Funding statement

This work was supported by Ministry of Education (MoE) Malaysia, HICoE Research Grant (R.J090301.7846.4J200) and Fundamental Research Grant Scheme (FRGS) (R.J130000.7846.4F981).

Competing interest statement

The authors declare no conflict of interest.

Additional information

No additional information is available for this paper.

References

[1] D. Golberg, Y. Bando, Y. Huang, T. Terao, M. Mitome, C. Tang, C. Zhi, Boron nitride nanotubes and nanosheets: review, Am. Chem. Soc. Nano 4 (2010) 2979−2993.

[2] R.K. Thines, N.M. Mubarak, S. Nizamuddin, J.N. Sahu, E.C. Abdullah, P. Ganesan, Application potential of carbon nanomaterials in water and wastewater treatment: a review, J. Taiwan Inst. Chem. Eng. 72 (2017) 116−133.

https://doi.org/10.1016/j.heliyon.2019.e01142

[3] C.S. Ong, P.S. Goh, W.J. Lau, N. Misdan, A.F. Ismail, Nanomaterials for biofouling and scaling mitigation of thin film composite membrane: a review, Desalination 393 (2016) 2–15.

[4] W. Lei, D. Portehault, D. Liu, S. Qin, Y. Chen, Porous boron nitride nanosheets for effective water cleaning, Nat. Commun. 1777 (2013) 1–7.

[5] Y. Chen, J. Zou, S.J. Campbell, G.L. Caer, Boron nitride nanotubes: pronounced resistance to oxidation, Appl. Phys. Lett. 84 (2004) 2430–2432.

[6] J. Li, J. Lin, X. Xu, X. Zhang, Y. Xue, J. Mi, Z. Mo, Y. Fan, L. Hu, X. Yang, J. Zhang, F. Meng, S. Yuan, C. Tang, Porous boron nitride with a high surface area: hydrogen storage and water treatment, Nanotechnology 24 (2013) 1–7.

[7] M.A. Rafiee, T.N. Narayanan, D.P. Hashim, N. Sakhavand, R. Shahsavari, R. Vajtai, P.M. Ajayan, Hexagonal boron nitride and graphite oxide reinforced multifunctional porous cement composites, Adv. Funct. Mater. 23 (2013) 5624–5630.

[8] L. Xue, B. Lu, Z. Wu, C. Ge, P. Wang, R. Zhang, X. Zhang, Synthesis of mesoporous hexagonal boron nitride fibers with high surface area for efficient removal of organic pollutants, Chem. Eng. J. 243 (2014) 494–499.

[9] J. Li, Y. Huang, Z. Liu, J. Zhang, X. Liu, H. Luo, Y. Ma, X. Xu, Y. Lu, J. Zou, C. Tang, Chemical activation of boron nitride fibers for improved cationic dye removal performance, J. Mater. Chem. A 3 (2015) 8185–8193.

[10] Ludovic Garnier, Szymczyk Anthony, Patrice Malfreyt, Ghoufi Aziz, Physics behind water transport through nanoporous boron nitride and graphene, J. Phys. Chem. Lett. 7 (2016) 3371–3376.

[11] M. Shahbabaei, D. Kim, Molecular dynamics simulation of transport mechanisms through nanoporous boron nitride and graphene multilayers, J. Phys. Chem. B 121 (2017) 4137–4144.

[12] M. Weber, B. Koonkaew, S. Balme, I. Utke, F. Picaud, I. Iatsunskyi, E. Coy, P. Miele, M. Belchelany, Boron nitride nanoporous membranes with high surface charge by atomic layer deposition, Appl. Mater. Interfac. 9 (2017) 16669–16678.

[13] Jafar Azamat, Batoul Shirforush Sattary, Alireza Khataeea, Sang Woo Joo, Removal of a hazardous heavy metal from aqueous solution using functionalized graphene and boron nitride nanosheets: insights from simulations, J. Mol. Graph. Model. 61 (2015) 13–20.

[14] Haiqi Gao, Shi Qi, Dewei Rao, Yadong Zhang, Jiaye Su, Yuzhen Liu, Yunhui Wang, Kaiming Deng, Ruifeng Lu, Rational design and strain

 https://doi.org/10.1016/j.heliyon.2019.e01142

engineering of nanoporous boron nitride nanosheet membranes for water desalination, J. Phys. Chem. C 121 (2017) 22105−22113.

[15] F. Mahvash, S. Eissa, T. Bordjiba, A.C. Tavares, T. Szkopek, M. Siaj, Corrosion resistance of monolayer hexagonal boron nitride on copper, Sci. Rep. 7 (2017) 42139., 1−5.

[16] Preeti Singla, Neetu Goel, Vinod Kumar, Sonal Singhal, Boron nitride nanomaterials with different morphologies: synthesis, characterization and efficient application in dye adsorption, Ceram. Int. 41 (2015) 10565−10577.

[17] K.H. Chu, Y. Huang, M. Yu, J. Heo, R.V.F. Joseph, A. Jang, M. Jang, C. Jung, C.M. Park, D. Kim, Y. Yoon, Evaluation of graphene oxide-coated ultrafiltration membranes for humic acid removal at different pH and conductivity conditions, Separ. Purif. Technol. 181 (2017) 139−147.

[18] Valeen Rashmi Pereira, Arun M. Isloor, A.K. Zulhairun, M.N. Subramaniam, W.J. Lau, A.F. Ismail, Preparation of polysulfone-based PANI−TiO_2 nanocomposite hollow fiber membranes for industrial dye rejection applications, RSC Adv. 6 (2016) 99764−99773.

[19] G. Arthanareeswaran, D. Mohan, M. Raajenthiren, Preparation, characterization and performance studies of ultrafiltration membranes with polymeric additive, J. Membr. Sci. 350 (2010) 130−138.

[20] P.V. Chai, E. Mahmoudi, Y.H. Teow, A.W. Mohammad, Preparation of novel polysulfone-Fe_3O_4/GO mixed-matrix membrane for humic acid rejection, J. Water Process Eng. 15 (2017) 83−88.

[21] Hui Li, Xiao Cheng Zeng, Wetting and interfacial properties of water nanodroplets in contact with graphene and monolayer boron nitride sheets, ACS Nano 6 (2012) 2401−2409.

[22] A.K. Zulhairun, A.F. Ismail, The role of layered silicate loadings and their dispersion states on the gas separation performance of mixed matrix membrane, J. Membr. Sci. 468 (2014) 20−30.

[23] Florian Bouville, Sylvain Deville, Dispersion of boron nitride powders in aqueous suspensions with cellulose, J. Am. Ceram. Soc. (2014) 1−5.

[24] R.R. Nair, H.A. Wu, P.N. Jayaram, I.V. Grigorieva, A.K. Geim, Unimpeded permeation of water through helium-leak−tight graphene-based membranes, Science 335 (2012) 442−444.

[25] Meng Hu, Baoxia Mi, Enabling graphene oxide nanosheets as water separation membranes, Environ. Sci. Technol. 47 (2013) 3715−3723.

 https://doi.org/10.1016/j.heliyon.2019.e01142

[26] B. Radha, A. Esfandiar, F.C. Wang, A.P. Rooney, K. Gopinadhan, A. Keerthi, A. Mishchenko, A. Janardanan, P. Blake, L. Fumagalli, M. Lozada-Hidalgo, S. Garaj, S.J. Haigh, I.,V. Grigoreva, H.A. Wu, A.K. Geim, Molecular transport through capillaries made with atomic-scale precision, Nature 538 (2016) 222−225.

[27] I. Christl, R. Kretzschmar, Relating ion binding by fulvic and humic acids to chemical composition and molecular size. 1. Proton binding, Environ. Sci. Technol. 35 (2001) 2505−2511.

[28] K.P.V. Lekshmi, S. Yesodharan, E.P. Yesodharan, MnO_2 efficiently removes indigo carmine dyes from polluted water, Heliyon 4 (2018), 1−52.

https://doi.org/10.1016/j.heliyon.2019.e01142